

Constrained Local Universe Simulations (CLUES)

Stefan Gottlöber, Yehuda Hoffman and Gustavo Yepes

Abstract The local universe is the best known part of our universe. Within the CLUES project (<http://clues-project.org> — Constrained Local Universe Simulations) we perform numerical simulations of the evolution of the local universe. For these simulations we construct initial conditions based on observational data of the galaxy distribution in the local universe. Here we review the technique of these constrained simulations. In the second part we summarize our predictions of a possible Warm Dark Matter cosmology for the observed local distribution of galaxies and the local spectrum of mini-voids as well as a study of the satellite dynamics in a simulated Local Group.

1 Introduction

During the last decade cosmological parameters have been determined to a precision of just a few percent giving rise to the standard model of cosmology: a flat Friedmann universe whose mass-energy content is dominated by a cosmological constant (the Λ term), a cold dark matter (CDM) component and baryons. The convergence to a standard model of cosmology sets the framework for studying the formation of both the large scale structure and of galaxies within that model. The main goal of this study is to achieve a physical understanding of how the observed structure emerged within the context of the given cosmological model. This model specifies

Stefan Gottlöber

Astrophysical Institute Potsdam, An der Sternwarte 16, 14482 Potsdam, Germany e-mail: sgottloeber@aip.de

Yehuda Hoffman

Racah Inst. of Physics Hebrew University Jerusalem 91904, Israel e-mail: hoffman@huji.ac.il

Gustavo Yepes Departamento de Física Teórica C-15; Universidad Autónoma de Madrid; Madrid 28049, Spain e-mail: gustavo.yepes@uam.es

the cosmological expansion history, the initial conditions and the material content of the universe. These plus the knowledge of the physical laws governing the dynamics of the dark matter, baryons and radiation provide the framework within which a successful model of galaxy formation can be developed.

The basic paradigm of structure formation in the Λ CDM was formulated more than 30 years ago [19]. It suggests that dark matter (DM) clusters to form DM halos, within which galaxy formation takes place via complex baryonic physics. Intensive numerical efforts of the last decade have validated the basic White & Rees picture. Yet, the process of galaxy formation is much more complicated than that simple picture. DM halos grow via process of mergers of substructures and galaxy formation proceeds by the combined action of clumpy and anisotropic gas accretion and mergers dwarf galaxies. As dwarf galaxies cross the virial radius of the DM halo they become satellites, subject to tidal forces exerted by the central potential. This transforms the satellites into tidal streams and eventually phase mixing dissolves the streams into the stellar halo of galaxies. This process manifests itself in the combined color and dynamical phase space of galactic stellar halos. This is the universal mode of galaxy formation but it can be observed and analyzed only in the very local universe, resulting in the so-called near-field cosmology. This motivates cosmologists to turn their attention and study the archeology of the Local Group (LG) in their quest for understanding galaxy formation. This also motivates us to simulate the formation of the LG in the most realistic possible way.

Cosmological simulations may cover a large dynamical and mass range. A representative volume of the universe should be large, but this comes at the expense of the mass resolution, which must be decreased in proportion to the simulated volume size. One may reduce the box size at the expense of possibly not being representative. To overcome this problem we use smaller simulation boxes specifically designed to represent the observed local universe. The algorithm of constrained realizations of Gaussian field provides a very attractive method of imposing observational data as constraints on the initial conditions and thereby yielding structures which can closely mimic those in the actual universe. The prime motivation of the CLUES project is to construct simulations that reproduce the local cosmic web and its key 'players', such as the Local Supercluster, the Virgo cluster, the Coma cluster, the Great Attractor and the Perseus-Pisces supercluster. The main drawback of current constrained simulations is that they do not directly constrain the sub-megaparsec scale structure, yet they enable the simulation of these scales within the correct environment. Such simulations provide a very attractive possibility of simulating objects with properties close to the observed LG and situated within the correct environment. Their random origin, however, limits the predictive power of the simulations and in particular the constraining power of our 'near field cosmology' experiments. It is one of our main goals to improve the constraining power and ability of the simulations to reproduce the actual observed LG.

2 Constrained Simulations

During the past few years we have performed a series of constrained simulations of the local universe. We continue this research to answer within the next generation of constrained simulations the question how unique the LG is. To this end we will use more and better observational data of the local Universe. Our main motivation is to use the constrained simulations as a numerical near-field cosmological laboratory for experimenting with the complex DM and gas physics processes.

2.1 *Observational Data*

Observational data of the nearby universe is used as constraints on the initial conditions and thereby the resulting simulations reproduce the observed large scale structure. The implementation of the algorithm of constraining Gaussian random fields [4] to observational data and a description of the construction of constrained simulations was described already elsewhere [10, 8]. Here we briefly describe the observational data used. Two different observational data is used to set up the initial conditions. The first is made of radial velocities of galaxies drawn from the MARK III [20], SBF [17] and the Karachentsev [6] catalogs. Peculiar velocities are less affected by non-linear effects and are used as constraints as if they were linear quantities [21]. The other constraints are obtained from the catalog of nearby X-ray selected clusters of galaxies [13]. Given the virial parameters of a cluster and assuming the spherical top-hat model one can derive the linear overdensity of the cluster. The estimated linear overdensity is imposed on the mass scale of the cluster as a constraint. For the CDM cosmologies the data used here constrains the simulations on scales larger than $\approx 5h^{-1}\text{Mpc}$ [8]. It follows that the main features that characterise the local universe, such as the Local Supercluster, Virgo cluster, Coma cluster and Great attractor, are all reproduced by the simulations. The small scale structure is hardly affected by the constraints and is essentially random.

2.2 *Constrained Initial conditions*

The Hoffman-Ribak algorithm [4] is used to generate the initial conditions as constrained realizations of Gaussian random fields on a 256^3 uniform mesh, from the observational data mentioned above. Since these data only constrain scales larger than a very few Mpc, we need to perform a series of different realizations in order to obtain one which contain an LG candidate with the correct properties (e.g. two halos with proper position relative to each-other, mass, negative radial velocity, etc). Hence the low resolution, 256^3 particle simulations were searched and the one with the most suitable Local Group like objects were chosen for follow up, high resolution re-simulations. We generated more than 200 realizations of these simulations

and all of them were evolved since the starting redshift ($z = 50$) till present time ($z = 0$) using the TREEPM N-body algorithm in GADGET2. We used 64 processors of HLRB2 Altix supercomputer and the typical wall clock time for each of them was of the order of 10 hours.

High resolution extension of the low resolution constrained realizations were then obtained by creating an unconstrained realization at the desired resolution, FFT-transforming it to k-space and substituting the unconstrained low k modes with the constrained ones. The resulting realization is made of unconstrained high k modes and constrained low k ones. In order to be able to zoom into the desired Local Group object, we set up the unconstrained realization to the maximum number of particles we can allocate in one node of the HLRB2 Altix cluster. Since our initial conditions generator code is OpenMP parallel, we can only run it in shared memory mode. Thus, thanks to the cc-NUMA architecture of the Altix, we can address as much as 2 Tbytes of RAM for an OpenMP program. This means we can accommodate as many as 4096^3 particles in this memory. We used up to 500 processors in one node and 1.5 Tbytes of memory for that. The typical cpu time per run is of the order of 5-6 hours wall clock. Most of this time was taken to generate the sequence of Gaussian random numbers, which was done in serial mode. We would not have been able to proceed in this project if we had not have access to this computer. In fact, there are very few architectures in the world with this huge amount of shared memory per node. We are now rewriting the initial condition generator code to MPI to overcome these limitations.

We did two different kind of initial conditions using the procedure described above. On one hand we were interested in simulating the large scale structures of the whole simulation box of $64h^{-1}\text{Mpc}$ with enough resolution to resolve halos which can be related with the dwarf galaxies in our real Universe. To this end, once we generated the initial conditions for the largest number of particles, (i.e. 4096^3) then we degraded them down to a maximum of 1024^3 in the whole box.

On the other hand, we were also interested in re-simulating with very high resolution the formation of the LG candidates found in the low resolution simulations. To this end, we re-simulate the evolution of this region of interest, using the full resolution (equivalent to 4096^3 effective particles) only within a sphere of just $2h^{-1}\text{Mpc}$. Outside this region, the simulation box is populated with lower resolution (i.e higher mass) particles. We were thus able to achieve high resolution in the region of interest, while maintaining the correct external environment. These initial conditions were set up at very high redshift ($z = 100$) to avoid spurious effects due to cell crossing in the high resolution volume. We then populate this volume with two different species, dark matter and SPH gas particles, for the case of running hydrodynamical simulations of these objects.

2.3 Description of Simulations

Using the above initial conditions, we carried out the simulations using the MPI N-body + SPH code GADGET2, developed by V. Springel[15]. The total amount of computing time that has been invested in all the experiments done within the CLUES collaboration has been tremendous. We had to distribute the work among different supercomputers in Europe, mainly the HLRB2 at LRZ, the MareNostrum at BSC, and JUMP and more recently Juropa at Jülich. In all cases, the initial conditions were always generated in HLRB2 at LRZ for the reasons explained above.

In total we have run 3 big collisionless (N-body only) simulations with 1 billion particles each (i.e. 1024^3), and 2 more are currently running. Two of these simulations correspond to one realization with WMAP3 cosmological parameters, that was done both assuming CDM and WDM with $m_{WDM} = 1$ keV and the other one is a CDM realization with WMAP5 cosmological parameters.

The simulations started at $z = 50$ and were evolved until $z = 0$. We stored of the order of 190 snapshots, 60 of them with very fine time interval of 15 million years between them, until $z = 6$. Then, we enlarged the time interval to 100 million years between consecutive snapshots. Since each snapshot is 32 Gbytes in size, we stored of the order of 6.1 Tbytes of data in each run. We used 500 MPI processors and the typical computing time needed for these runs was of the order of 130-150k CPU hours.

The other set of simulations we have also performed correspond to the re-simulations of the LG object found in two of the constrained realizations. As explained above, we have re-simulated a sphere with a radius of $2h^{-1}$ Mpc around the object position at present time, with the maximum resolution allowed by our initial condition setting (i.e. 4096^3 effective particles in the re-simulate volume). We use the same set of initial conditions to run two simulations, one with dark matter only and another one with dark matter, gas dynamics, cooling, star formation and supernovae feedback. In our SPH simulation, each high resolution dark matter particle was replaced by an equal mass, gas - dark matter particle pair with a mass ratio of roughly 1:5.

Due to the strong clustering of the objects formed in these simulations, the GADGET code does not scale very well with number of processors. Thus, we decided to use the minimum necessary to allocate all the data into memory. Total number of particles in these simulations are of the order of 130-150 million. On HLRB2 Altix at LRZ we have used 64 to 128 processors for these runs. The total amount of cpu time exceeded the computational resources allocated in normal projects, so we used also most of the time that was granted to us from DEISA Extreme Computing Initiative (DECI) in two consecutive projects named, SIMU-LU and SIMUGAL-LU. Each of them consistent of 1 million cpu hours divided among MareNostrum and HLRB2. We also benefited from the DEISA high speed network in order to transfer the snapshots between the two centres.

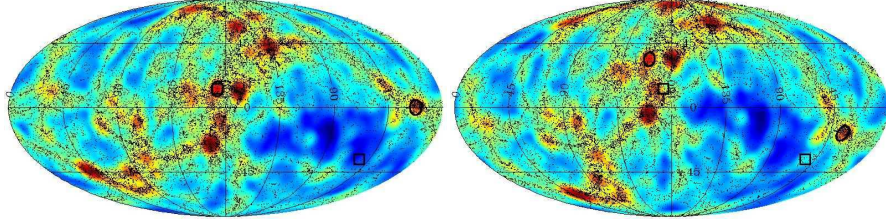


Fig. 1 The left and the right plot show two projected sky maps with halos up to a distance of $20h^{-1}\text{Mpc}$ from the simulated Milky Way (see text for an explanation of the used coordinate system).

Simulations of the full box

To find a LG candidate we first identify in the constrained simulation the Virgo cluster. Then we search for an object which closely resembles the Local Group and is in the right direction and distance to Virgo. Based on the locations of the LG and Virgo we now define a coordinate system similar to the super-galactic coordinate system. We assume that the equatorial plane of the super-galactic coordinate system lies in the super-galactic plane, which is spanned by the Local Group and the Local Supercluster. Thus we need another object besides Virgo to define this plane. As shown by Zavala et al [22] the Ursa Major cluster is a natural choice. Rotating the coordinate system until the simulated Virgo cluster is at the same angular position as the observed one we have fixed our coordinate system. This coordinate system is visualised in the left panel of Fig. 1 which shows a sky map with the angular distribution of halos within $20h^{-1}\text{Mpc}$ from the simulated Milky Way in equatorial coordinates (RA, DEC) in a Mollweide projection. Here the value of each pixel is given by a mass-weighted count of all halos located in that pixel (high density: red, low density: blue) and all halos with masses larger than $5 \times 10^9 h^{-1} M_{\odot}$ appear as black points (see [22] for details).

The simulated Local Supercluster can be seen as prominent vertical structure in the left panel of Fig. 1. By construction the simulated Virgo cluster (black circle) and the real one (black square) are at the same position in the centre of the plot. However, the simulated position (black circle on the right edge of the plot) of a second nearby cluster, Fornax, differs from its observed position (the black square). Such deviations are within the expected variations of the constrained simulations. In fact, small scale structure (as the position of the local group) are not constrained by the observational data. The sky maps shown in Fig. 1 depend obviously of the chosen origin (MW). The situation can be improved by an additional adjustment of the coordinate system. One can relax the requirement that the angular position of the simulated and real Virgo has to coincide and use a coordinate system that minimises the quadratic sum of the distances between the simulated and real clusters Virgo and Fornax (Fig. 1, right panel).

Zoomed Simulations of the Local Group

On the left panel of Fig. 2 the gas distribution in the Local Group is shown. The size of the plot is about $2h^{-1}\text{Mpc}$ across, viewed from a distance of $3.3h^{-1}\text{Mpc}$. On the three right panels we show the gas disks of the three main galaxies as seen from a distance of $250h^{-1}\text{kpc}$, the size of the plot is about $50h^{-1}\text{kpc}$. Since the three disks are seen from the same distance and direction one can evaluate the relative orientation of the three gas disks. Note, that the M31 and MW disks are smaller than the disk of M33 due to major mergers which these objects had recently ($\sim z = 0.6$). In the section 2.4 we have described the new realizations of the local group which do not show such recent major mergers.

The images were rendered with A. Khalatyan’s SPMViewer using the remote visualisation server RVS1 at LRZ. This allowed us to render the particles directly on the GPU, which took one to two minutes per frame when using all 52 million gas particles of the high resolution region. We chose a logarithmic colour table for visualising the density distribution of the gas: dark colours for low density and bright colours for high density regions. The colours and density range are adjusted such that the faint structures and filaments connecting the three main galaxies become visible. For the zoomed images we shifted the density range for colour mapping by a factor of $10^{0.5}$ in order to improve the contrast and to enhance the spiral arm features of the gas disks.

2.4 An Ensemble of Constrained Simulations

As we explained above, we generated an ensemble of 200 constrained simulations within the framework of the WMAP5 cosmological model. These low resolution simulations have been inspected to find suitable Local Group like objects. Typically 10 such objects fulfil our selection criteria [12] in a volume of $(64 h^{-1}\text{Mpc})^3$. However, these objects are not necessarily located close to the actual location of the Local Group, namely nearby and in the right direction of the the simulated Virgo cluster and the Local Supercluster. In addition to the LG identified in the WMAP3 simulation (see Fig. 2) we have identified five more objects which allow us to study the scatter in the properties of these ”Local Groups”.

Moreover, the ensemble of 200 constrained simulations can be used to study the statistical properties of the linear constrained realizations, the non-linear density and velocity fields extracted from the simulations, and the relation between the constrained initial conditions and the final simulations. A first step in this direction is presented here. A sub-ensemble of 60 linear constrained realizations is studied and the mean and the variance of the linear density and velocity fields are studied. Fig. 3 presents the mean, taken over the 60 constrained realizations, of the density (left panel) and the three-dimensional velocity fields. The presented velocity field corresponds to the divergent component of the velocity field which is constructed by removing the tidal component which is produced by the

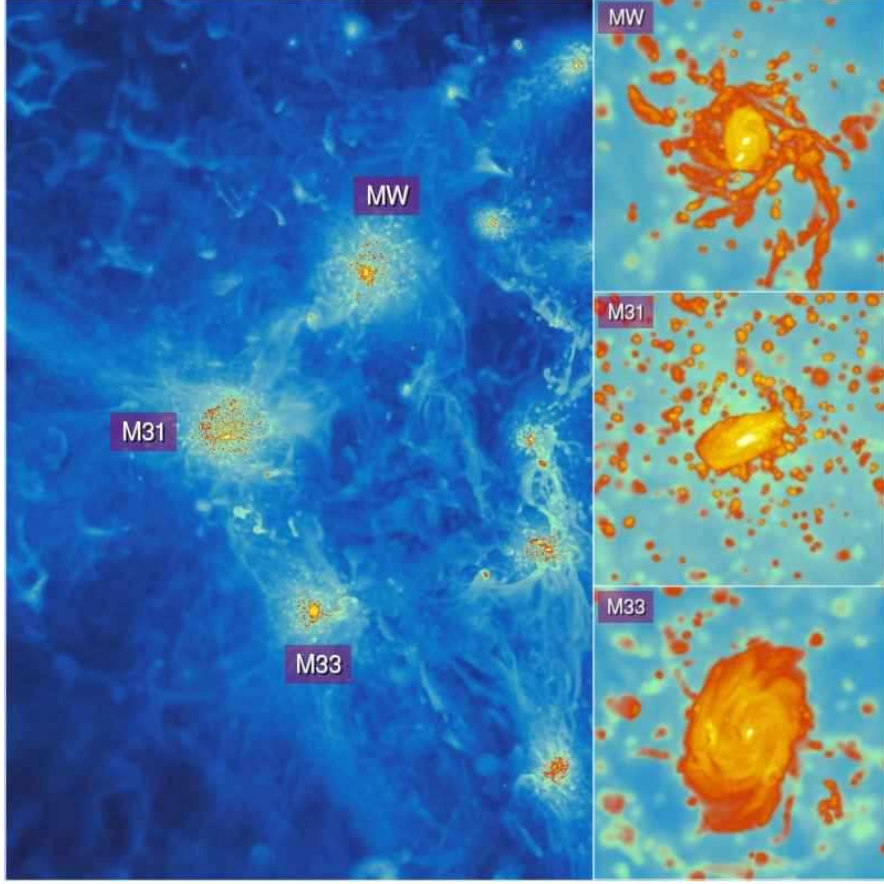


Fig. 2 The left hand side of the plot shows the gas distribution in the Local Group. On the right hand side we zoom on the three objects (MW, M31, M33)

mass distribution outside the computational box[5]. The cosmography exhibited by the constrained realizations is dominated by the Local Supercluster, running at roughly $SGY \approx 15h^{-1}\text{Mpc}$ across the box, and in particular by the Virgo cluster at $[SGX, SGY, SGZ] \approx [-8, 15, 0]h^{-1}\text{Mpc}$. Note that linearly recovered Virgo cluster is already shifted by a few Mpc to the left on the Supergalactic plan. The velocity field itself converges close to $\approx [-20, 10, 0]h^{-1}\text{Mpc}$, and therefore we expect to see a drift of the simulated Virgo in the negative SGX direction.

Fig. 3 shows the mean density and velocity fields, however individual constrained realizations deviate from the mean. To study the nature of the scatter of the constrained realizations from the mean field we calculate the scatter, i.e. the standard deviation, of the density field. It is interesting to see how robust are the various features uncovered by the constrained realizations against the scatter exhibited by the constrained realizations. Fig. 4 presents the mean density field divided by the lo-

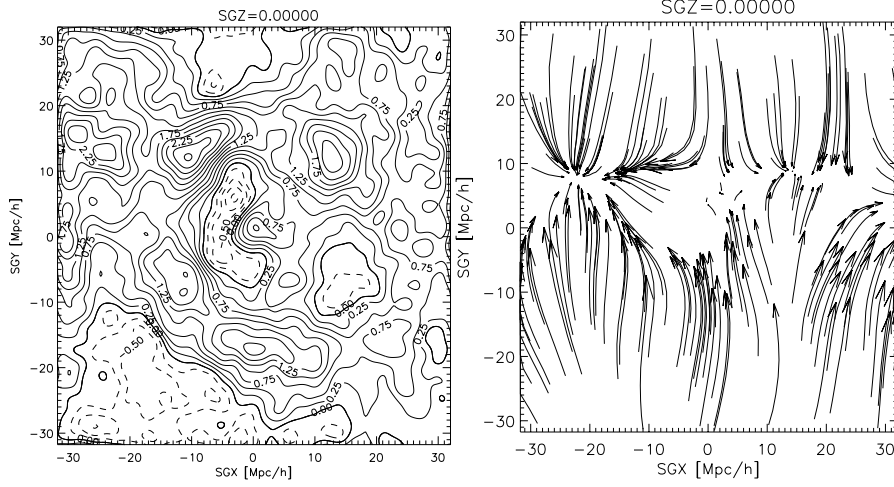


Fig. 3 The mean linear density and velocity fields. Left: linear density field smoothed by a Gaussian kernel with $R_g = 1 h^{-1} \text{Mpc}$, solid, solid thick and the dashed lines correspond to positive, zero and negative values. Right: velocity field

cal scatter. This normalization of the field by "sigma" is strongly scale dependent. A Gaussian kernel of $R_g = 5 h^{-1} \text{Mpc}$ is used in the left panel and $R_g = 1 h^{-1} \text{Mpc}$ in the right one. Normalizing the mean field by the local scatter provides a local measure of the statistical significance of any feature recovered by the constrained realizations. The figure shows that indeed the Local Supercluster is the most robust feature of the constrained realizations. Yet, the normalized $R_g = 1 h^{-1} \text{Mpc}$ map is almost featureless with typical values of around unity. It follows that the $\approx 1 h^{-1} \text{Mpc}$ structure is virtually unconstrained by the imposed data, within the WMAP5 cosmology adopted here, whereas scales larger than roughly $5 h^{-1} \text{Mpc}$ are strongly constrained by the data.

3 Latest results from CLUES simulations

Within our project at the Leibniz Rechenzentrum we have performed a series of constrained simulations with 1 billion particles in boxes of $160 h^{-1} \text{Mpc}$ as well as $64 h^{-1} \text{Mpc}$ side length using both GADGET and ART. Moreover, we have re-simulated an object which closely resembles our local group with different resolutions as well as different physics. In the following two subsections we summarise a few of the most interesting results.

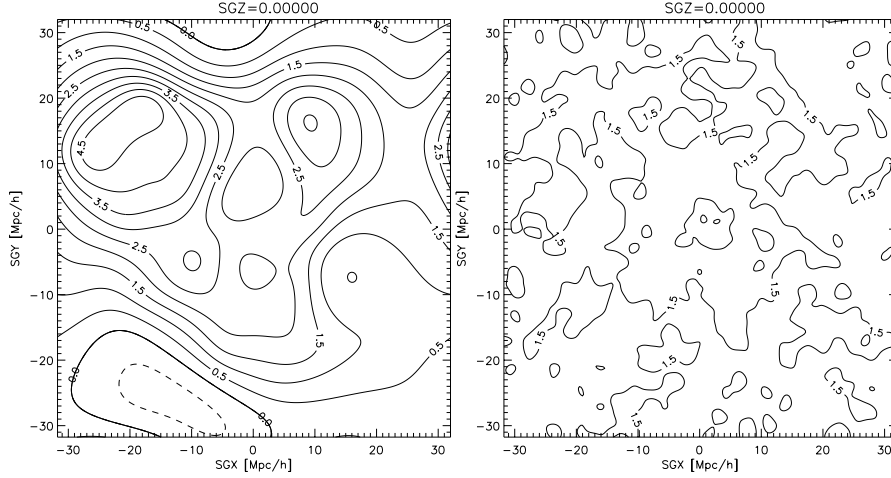


Fig. 4 Left: The scatter, i.e the standard deviation, around the mean density field smoothed by a Gaussian kernel with $R_g = 5h^{-1}\text{Mpc}$ is evaluated. The figure shows the mean density field normalised by its scatter. Right: The same but for $R_g = 1h^{-1}\text{Mpc}$.

3.1 Warm Dark Matter in the local Universe

We have performed a series of constrained simulations with 1024^3 dark matter particles assuming the WMAP3 normalization of the power spectrum[14]: $\Omega_m = 0.24$, $\Omega_\Lambda = 0.76$, $H_0 = 100h \text{ km s}^{-1} \text{ Mpc}^{-1}$ with $h = 0.73$, $n = 0.95$ and $\sigma_8 = 0.75$. In order to test the effects of different dark matter candidates in the structure of the local groups, we also generated the same initial conditions but assuming that the dark matter is made of a warm, low mass candidate with a mass per particle of $m_{\text{WDM}} = 1 \text{ keV}$. The effects of Warm Dark Matter (WDM) on the structure formation is to remove power from short scales, due to the large thermal velocities of the particles. For such WDM particles the free-streaming length is $350h^{-1}\text{kpc}$ which corresponds to a filtering mass of $\sim 1.1 \times 10^{10}h^{-1}\text{M}_\odot$ [1]. Thus, we just had to change the initial power spectrum, from the standard CDM, to the WDM which contains a sharp cut-off at the free-streaming length. In order to test the effect of the WDM on the structures formed, we need to have enough mass resolution to resolve those structures well below the cut-off imposed by the free streaming of WDM particles. This translates into a minimum number of particles in a simulation box such that the Nyquist Frequency imposed by the discreteness of our sampling of particles, be always smaller than the frequency at the cut-off in the WDM spectrum. Using 1024^3 particles in the simulation box, we ensure that this conditions fulfils. Thus, we generated the same realization for both CDM and WDM constrained initial conditions

In a universe filled with Warm Dark Matter the exponential cut-off in the power spectrum leads naturally to a reduction of small scale structure. Our choice of $m_{\text{WDM}} = 1 \text{ keV}$ is close to the lower limit for the mass of the WDM particle pre-

dicted by observations. We have chosen this extreme case to study the maximal possible effect of the Warm Dark Matter on the local structure of the universe as discussed in more detail in Zavala et al [22] and Tikhonov et al [16]. We summarize here the main results from the analysis of the big simulations with 1024^3 dark matter particles assuming the WMAP3 normalization of the power spectrum [14] and two model WDM and CDM that were described in the previous sections.

In the Λ CDM case the mass function of halos in the whole simulated box follows closely the estimates from the Sheth & Tormen formalism, except in the highest mass end due to the influence of the Local Supercluster, a massive structure in this small box which comes in due to the observational constraints. In the Warm Dark Matter universe the mass function lies close to the CDM one for halos with masses higher than the filtering mass, however for lower masses it flattens and then rise due to spurious numerical fragmentation for masses $\lesssim 3 \times 10^9 h^{-1} M_\odot$ [18]. The mass resolution of $m_{\text{DM}} = 1.63 \times 10^7 h^{-1} M_\odot$, allows us to derive robust results for halos with masses larger than this limiting mass, corresponding to maximum rotation velocities of 24 km s^{-1} .

From the Warm and Cold Dark Matter simulations we have calculated the velocity functions of haloes which has the advantage over the mass function that it can be compared more directly with observational data. From our simulations we have obtained predictions for the velocity function of halos in the field of view, within $20 h^{-1} \text{ Mpc}$, that is being surveyed by the ongoing Arecibo Legacy Fast ALFA (ALFALFA) HI blind survey [2, 3]. This survey is divided into two regions on the sky, one includes the Virgo cluster, the other points into the opposite direction. Additionally constrained to distances less than $20 h^{-1} \text{ Mpc}$ we call these here the “Virgo-direction region” and “anti-Virgo-direction region”, respectively. Zavala et al. [22] compared the constrained simulations with the ALFALFA observational data. The results are summarised in Fig.5.

For velocities in the range between 80 km s^{-1} and 300 km s^{-1} , the velocity functions predicted for the Λ CDM and Λ WDM simulations agree quite well with the observed velocity functions. This result is encouraging because it confirms that our constrained simulations properly reflect our local environment. In fact, the simulations are able to predict the shape and normalization of the velocity function in the high velocity regime, in particular in the Virgo direction, where the normalization is an order of magnitude larger than for the universal velocity function.

The minimum mass for which we can trust the simulations and observations corresponds to a maximum circular velocity of $\sim 35 \text{ km s}^{-1}$ (solid line in Fig. 5). Between this velocity and about $V_{\text{max}} \sim 80 \text{ km s}^{-1}$ the predictions agree well for the Λ WDM cosmogony. On the contrary, the Λ CDM model predicts a steep rise in the velocity function towards low velocities. Thus, at our limiting circular velocity, $V_{\text{max}} \sim 35 \text{ km s}^{-1}$, it forecasts ~ 10 times more sources both in Virgo-direction (red) as well as in anti-Virgo-direction (blue) than the ones observed by the ALFALFA survey. These results indicate a potential problem for the cold dark matter paradigm [22]. The spectrum of mini-voids also points to a potential problem of the Λ CDM model [9]. The Λ WDM model provides a natural solution to this problem, however,

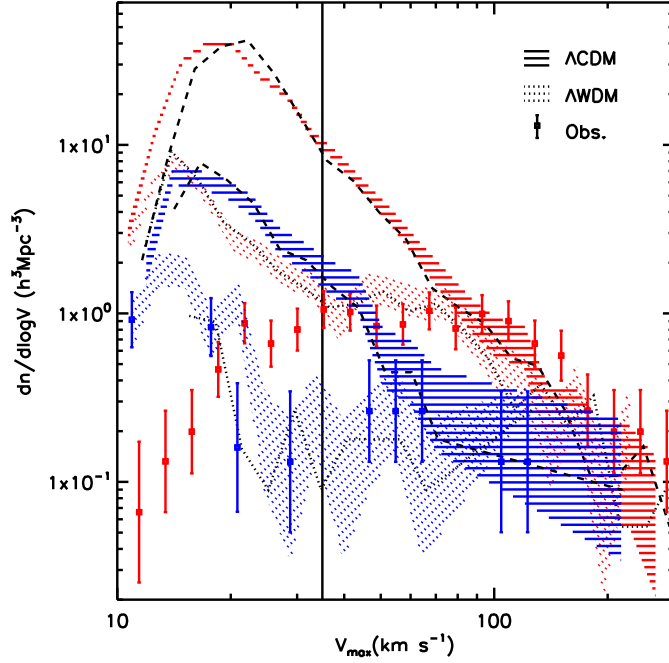


Fig. 5 Velocity function for the sample of galaxies in the Virgo-direction region taken from the ALFALFA catalogs (red square symbols with error bars). Predictions from our constrained simulations for the observed field of view appear as the dashed (Λ CDM) and dotted (Λ WDM) red areas, delimited by Poisson error bars. In blue the same is shown for the anti-Virgo-direction. The vertical solid line marks the value of V_{max} down to which the simulations and observations are both complete.

the late formation of halos in the Λ WDM model might be a problem for galaxy formation[16].

3.2 Satellites in the Local Group

Klimontowski et al. used the dark matter only zoomed simulation of the Local Group with an effective resolution of 4096^3 particles as a numerical laboratory for studying the evolution of the population of its sub-haloes[7]. In M31 they have detected a large group of in-falling satellites which consists of 30 haloes. Fig. 6 shows the orbits of the satellites projected on to the sky. The observer was placed in the centre of M31 and the coordinate system was chosen so that the z -axis is aligned with the angular momentum of M31. About 4 Gyrs ago the satellites fell into M31 from one well-defined region in the sky but the spread increases with time. This example

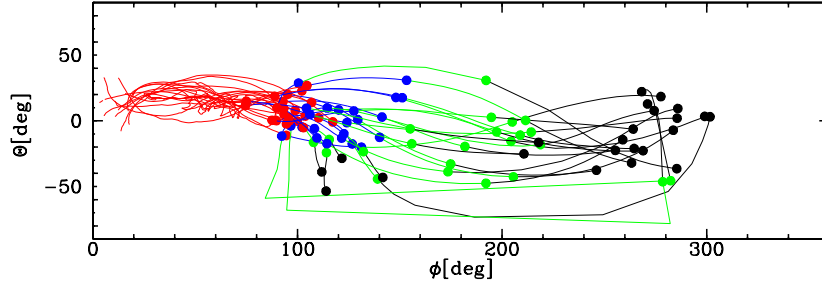


Fig. 6 Orbits of the large in-falling group of sub-haloes as seen by the observer placed at the centre of M31. The spherical coordinate system was aligned to match the angular momentum vector of the host which is pointing along the z axis. Different colours correspond to different times. Red circles: 3 Gyrs ago, blue: 2 Gyrs ago, green: 1 Gyr ago, black: present time.

suggests that the alignment of angular moments of in-falling satellites is not well conserved, even though the group has not yet decayed. One should thus be very careful when trying to reproduce the histories of dwarf galaxies using their present proper motions.

Since we were running simulations of the LG with and without baryons modelled hydrodynamically we can quantify the effect of gas physics on the $z = 0$ population of sub-haloes. We found [11] that above a certain mass cut, $M_{\text{sub}} > 2 \times 10^8 h^{-1} M_{\odot}$ sub-haloes in gas-dynamic simulations are more radially concentrated than those in in dark matter only simulations. The increased central density of such sub-halos results in less mass loss due to tidal stripping than the same sub-halo simulated with only dark matter. The increased mass in hydrodynamic sub-haloes with respect to dark matter ones causes dynamical friction to be more effective, dragging the sub-halo towards the centre of the host. In Fig. 7 we show as an example the mass and radial position of an in-falling satellite as a function of time. The same satellite has been identified in the dark matter only simulation (blue) and the gas-dynamical simulation (red). In the left panel one can see that the sub-halo's mass in the dark matter only simulation closely follows the SPH sub-halo's mass for a short period directly after accretion. However, by $z = 0.4$ the DM halo has already lost a good $\sim 10\%$ more than its SPH counterpart. By $z = 0$ the DM sister has lost $\sim 65\%$ of its infall mass, while the SPH sub-halo has only lost $\sim 45\%$ of its infall mass. In the right panel we show the orbit of this sub-halo as a function of redshift which diverge shortly after infall. By the first pericentric passage, the SPH sub-halo penetrates further in by about a factor of 2 than the DM sister. The sub-halo from the dark matter only simulation is consistently further behind the SPH sub-halo at all stages of the orbit, resulting in the SPH sub-halo being nearly a factor of 2 closer to the host halo's centre than the DM sub-halo at $z = 0$.

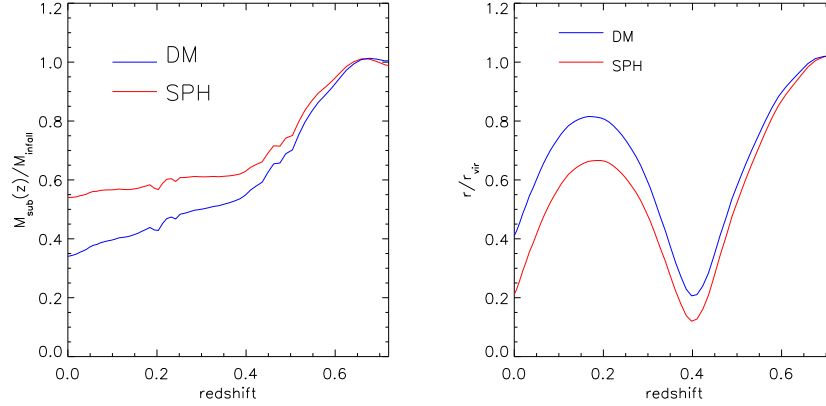


Fig. 7 Left: The mass of an SPH sub-halo (red line) and its DM sister (blue line) as a function of redshift, normalised to the mass each sub-halo had at infall, around $z = 0.72$. Right: The distance from the main halo of an SPH sub-halo and its DM sister as a function of redshift.

4 Summary

Within the CLUES project (<http://clues-project.org>) we have performed a series of constrained simulations of the local universe. These simulations reproduce the observed large scale structures around the Local Group whereas small scale structures below scales of $\sim 1h^{-1}\text{Mpc}$ are essentially random. In four simulations we have identified Local Groups situated at the right position but having different merging histories. Constrained simulations are a useful tool to study the formation and evolution of our Local Group in the right cosmological environment and the best possible way to make a direct comparison between numerical results and observations, minimizing the effects of the cosmic variance.

Acknowledgements The computer simulations described here have been performed at LRZ Munich and BSC Barcelona. We acknowledge support by ASTROSIM, DFG, DEISA and MICINN (Spain) for our collaboration. We thank Jesus Zavala (Munich), Noam Libeskind (Potsdam), Jarek Klimentowski (Warsaw) and Kristin Riebe (Potsdam) for providing plots from our common research projects.

References

1. Bode, P., Ostriker, J. P., & Turok, N. 2001, ApJ, 556, 93
2. Giovanelli, R., Haynes, M. P., Kent, B. R., Perillat, P., Catinella, B., Hoffman, G. L., Momjian, E., Rosenberg, J. L., & et al., 2005, AJ, 130, 2613
3. Giovanelli, R., Haynes, M. P., Kent, B. R., Saintonge, A., Stierwalt, S., Altaf, A., Balonek, T., Brosch, N., & et al., 2007, AJ, 133, 2569

4. Hoffman Y., Ribak E., 1991, *ApJL*, 380, L5
5. Hoffman Y., A. Eldar A., Zaroubi S., Dekel A., 2001, *astro-ph/0102190*
6. Karachentsev I. D., Karachentseva V. E., Huchtmeier W. K., Makarov D. I., 2004, *AJ*, 127, 2031
7. Klimontowski J., Lokas E.L., Knebe A., Gottlöber S., Martinez-Vaquero L. A., Yepes G., Hoffman Y., 2010, *MNRAS*, 402, 1899
8. Klypin A., Hoffman Y., Kravtsov A. V., Gottlöber S., 2003, *ApJ*, 596, 19
9. Klypin A., Tikhonov A., 2009, *MNRAS*, 395, 1915
10. Kravtsov, A. V., Klypin, A., & Hoffman, Y. 2002, *ApJ*, 571, 563
11. Libeskind N.I., Yepes G., Knebe A., Gottlöber S., Hoffman Y., Knollman S.R., 2010, *MNRAS*, 401, 1889
12. Martinez-Vaquero L.A., Yepes G., Hoffman Y., Gottlöber S., Sivan M., 2009, *MNRAS*, 397, 2070
13. Reiprich T. H., Böhringer H., 2002, *ApJ*, 567, 716
14. Spergel, D. N., Bean, R., Doré, O., Nolta, M. R., Bennett, C. L., Dunkley, J., Hinshaw, G., Jarosik, N., & et al., 2007, *ApJS*, 170, 377
15. Springel, V. 2005, *MNRAS*, 364, 1105
16. A.V. Tikhonov, S. Gottlöber, G. Yepes, Y. Hoffman, 2009, *MNRAS*, 399, 1611
17. Tonry J. L., Dressler A., Blakeslee J. P., Ajhar E. A., Fletcher A. B., Luppino G. A., Metzger M. R., Moore C. B., 2001, *ApJ*, 546, 681
18. Wang, J. & White, S. D. M. 2007, *MNRAS*, 380, 93
19. White S. D. M., & Rees M. J. 1978, *MNRAS*, 183, 341
20. Willick J. A., Courteau S., Faber S. M., Burstein D., Dekel A., Strauss M. A., 1997, *ApJ*, 109, 333
21. Zaroubi S., Hoffman Y., Dekel A., 1999, *ApJ*, 520, 413
22. J. Zavala, Y. P. Jing, A. Faltenbacher, G. Yepes, Y. Hoffman, S. Gottlöber and B. Catinella, 2009, *ApJ*, 700, 1779